Field Effect in Graphene-Based van der Waals Heterostructures: Stacking Sequence Matters

Stacking Sequence Matters

Stradi, Daniele; Papior, Nick Rübner; Hansen, Ole; Brandbyge, Mads

Published in:
Nano Letters

Link to article, DOI:
10.1021/acs.nanolett.7b00473

Publication date:
2017

Document Version
Peer reviewed version

Field effect in graphene-based van der Waals heterostructures: Stacking sequence matters

Daniele Stradi,[*,†,‡] Nick R. Papior,[†,¶] Ole Hansen,[§] and Mads Brandbyge[†]

Center for Nanostructured Graphene (CNG), Department of Micro- and Nanotechnology (DTU Nanotech), Technical University of Denmark, DK-2800, Kgs. Lyngby, Denmark, QuantumWise A/S, Fruebjergvej 3, Postbox 4, DK-2100 Copenhagen, Denmark, ICN2 - Institut Català de Nanociència i Nanotecnologia, Campus UAB, 08193 Bellaterra, Spain, and Department of Micro- and Nanotechnology (DTU Nanotech), Technical University of Denmark, DK-2800, Kgs. Lyngby, Denmark

E-mail: daniele.stradi@quantumwise.com

Abstract

Stacked van der Waals (vdW) heterostructures where semi-conducting two-dimensional (2D) materials are contacted by overlayed graphene electrodes enable atomically-thin, flexible electronics. We use first-principles quantum transport simulations of graphene-contacted MoS_2 devices to show how the transistor effect critically depends on the stacking configuration relative to the gate electrode. We can trace this behavior to the stacking-dependent response of the contact region to the capacitive electric field induced by the gate. The contact resistance is a central parameter and our observation establishes an important design rule for ultra-thin devices based on 2D atomic crystals.

[*]To whom correspondence should be addressed
[†]CNG – DTU Nanotech
[‡]QuantumWise
[¶]ICN2
[§]DTU Nanotech

Keywords

vdW heterostructures, field-effect, transport, graphene, density functional theory, non-equilibrium Green's function

Main Text

The recent advances in fabrication of heterostructures composed of stacks of atomically-thin layers bonded by van der Waals forces hold promise for ultra-thin electronics.[1–4] A key-idea is to use the semi-metallic graphene (G) as an electrode material to contact a 2D-semiconductor (2D-S) by a van der Waals bonded overlay region. A broad range of functional devices have been fabricated in this way including 2D field effect transitors (2D-FETs),[5–8] non-volatile memory cells,[9] photoresponsive memory devices,[10] and vertical tunneling FETs (V-TFETs).[11]

The contact resistance due to the van der Waals gap and Schottky barrier between graphene and the 2D-S is, however, critical for device performance. Opposed to conventional 3D metallic electrodes, the graphene work function (W_{G}) and density of carriers (n_{G}) are highly susceptible to external electric fields.[12,13] As a result, in a gated 2D-S/G device both the graphene electrodes as well as the 2D semiconductor are affected by the gate field $\vec{E}_{\mathrm{gate}}$, so the contact characteristics ultimately depend on the collective response of the 2D stack to $\vec{E}_{\mathrm{gate}}$. An emblematic example is that of devices with contacts based on graphene and MoS_2. Here several reports have observed a tunable contact resistance from rectifying to Ohmic by using increasingly positive gate voltages.[5–9] In particular, linear source-drain current (I_{SD}) *vs.* voltage (V_{SD}) characteristics, indicating the formation of an Ohmic contact between graphene and MoS_2, have been observed in independent measurements at gate voltages $\mathrm{V_{gate}} \geq 80$ V.[5,6] Such behaviour has been associated with the modulation of the Schottky barrier at the contact induced by $\vec{E}_{\mathrm{gate}}$.[5–7]

The experimental results have been obtained with structurally different device archi-

tectures. In some setups the MoS_2 is sandwiched in between the graphene and the gate electrodes (gate/MoS_2/G setup),[5,7,8] whereas in others the graphene is positioned below the MoS_2, in close proximity of the gate (MoS_2/G/gate setup).[6,9] While no apparent reason has been given for choosing one setup over the other, it has been argued that partial screening of $\vec{E}_{\text{gate}}$ by MoS_2 in gate/MoS_2/G setups may lead to a larger contact barrier.[6] The screening of $\vec{E}_{\text{gate}}$ by MoS_2 was also used to explain the saturation of I_{SD} with V_{gate} in vertical devices using a gate/MoS_2/G setup.[10] Although these conclusions are mostly based on simplified phenomenological models, there is growing evidence from theoretical analyses that more realistic approaches are needed to fully understand the field effect in graphene-based devices[14] and heterostructures.[15] This calls for a systematic characterization of the stacking-dependent response of the contact between graphene and 2D-SCs in 2D-FETs.

Here we use first principles electron transport calculations based on density functional theory combined with non-equilibrium Green's functions (DFT-NEGF) to investigate the transconductance of a MoS_2/G 2D-FET device. We show how the stacking sequence matters: We find a significantly higher transconductance for a gate/MoS_2/G device setup compared to a MoS_2/G/gate one. The effect can be explained by considering the different screening characteristics of the two materials forming the contact. In the MoS_2/G/gate setup, the influence of $\vec{E}_{\text{gate}}$ on the MoS_2 work function (W_{MoS_2}) is relatively small due to the good screening properties of doped graphene. On the other hand, in the gate/MoS_2/G setup the MoS_2 is fully exposed to $\vec{E}_{\text{gate}}$, leading to a stronger dependence of W_{MoS_2}, and consequently, a stronger dependence of the Schottky barrier on gating. Our findings can be summarized in a simple capacitor model.

The finite bias transconductance calculations have been performed using the TranSiesta[16,17] DFT-NEGF code, and the heterostructure corresponding to the device electrodes has been calculated using the Siesta[18] DFT code (see the Methods section). The gating has been accounted for by introducing a planar region with a uniform charge distribution (charge gate, CG).[14] The associated Poisson equation used to obtain the Hartree term V_{H}

in the DFT and DFT-NEGF Hamiltonians is

$$\nabla^2 V_{\mathrm{H}}(\mathbf{r}) = -\frac{\rho_{\mathrm{S}}(\mathbf{r}) + \delta\rho_{\mathrm{S}}(\mathbf{r}) - \delta\rho_{\mathrm{G}}(\mathbf{r})}{\epsilon_0}, \tag{1}$$

where $\rho_{\mathrm{S}}(\mathbf{r})$, $\delta\rho_{\mathrm{S}}(\mathbf{r})$, $\delta\rho_{\mathrm{G}}(\mathbf{r})$ and ϵ_0 are the electronic density of the non-gated system, the electronic density induced in the system by the gate, the corresponding counter-charge in the gate plane, and the vacuum permittivity. In order to access the CG method and the role of a dielectric screening inside the stack we performed additional calculations using the Atomistix ToolKit package[19] (see the Methods section). In this case, the gate has been described by introducing a spatial region of constant $V_{\mathrm{H}}(\mathbf{r})$ (Hartree gate, HG). We modelled the encapsulating dielectric (diel.) layer by including a second spatial region in which the local Hartree potential $V_{\mathrm{H}}^{\mathrm{diel.}}(\mathbf{r})$ is determined from

$$\nabla^2 V_{\mathrm{H}}^{\mathrm{diel.}}(\mathbf{r}) = -\frac{\rho_{\mathrm{S}}(\mathbf{r})}{\kappa}. \tag{2}$$

In the HG+diel. calculations, the dielectric permittivity has been set to $\kappa = 4\epsilon_0$ to mimic encapsulation in an hBN stack.

Our central device is shown in Fig. 1. We consider semi-infinite MoS_2/G overlay regions as electrodes to a MoS_2 channel. We have considered device setups in which electron transport occurs either along the zig-zag (ZZ) or the armchair (AC) directions of graphene and MoS_2, with the graphene terminations being AC or ZZ H-passivated graphene edges, respectively. Here we show only results for the AC transport direction, as similar conclusions are reached also for the ZZ case (see Fig. S1 in the Supporting Information). The MoS_2/G overlay structure is based on a 4×4/5×5 hexagonal supercell in which the graphene is strained isotropically by 2.11% and the MoS_2 is kept at its equilibrium lattice constant (a_{MoS_2}= 3.16 Å). It has been shown that for comparable strains applied to the graphene, the Dirac cone remains intact, the Fermi velocity changes by less than 5% and the work function by less than 0.2 eV.[20] The interlayer distance is 3.25 Å, as obtained from accurate plane-waves

calculations using the DFT-D2/PBE method[21,22] (see the Methods section). This value is comparable to that of 3.4 ± 0.1 Å reported by recent scanning high-resolution transmission electron microscopy measurements[23] and to the value of 3.32 Å obtained in earlier calculations for similar MoS_2/G heterostructures,[24] with small differences due to the different computational parameters employed (see the Methods section). Using the CG method, the charge in the device can be modulated by a gate electrode situated either below it (bottom gate, BG) or above it (top gate, TG), covering the whole structure. The former and the latter device setups corresponds to a gate/MoS_2/G and a MoS_2/G/gate contact geometry, respectively. We did not consider different arrangements of the graphene atoms over MoS_2 as previous calculations reported in the literature have shown how the electronic properties of the MoS_2/G heterostructure are rather insensitive to lateral displacements.[24]

In Fig. 2a we show the calculated I_{SD} for an applied bias of $V_{SD} = 0.2$ V. In agreement with experimental observations[5–7], I_{SD} increases considerably when an electron doping charge (n_d) is induced in the device by the gate – Notice that overall charge neutrality requires that $n_d = n_G + n_{MoS_2}$, with n_{MoS_2} being the charge localized on the MoS_2 layer. However, the most striking feature is that the magnitude of I_{SD} differs significantly depending on the active gate. For the TG device setup, where the graphene overlaying electrode is closer to the gate, we observe markedly smaller currents compared to the BG device setup. The ratio $I_{SD}(BG)/I_{SD}(TG)$ increases steadily with n_d, reaching a factor of 5000 at $n_d = 10.8 \times 10^{12}$ cm^{-2}, which corresponds to a doping density comparable to the highest ones reached experimentally.[5] Looking at the corresponding transmission functions for the representative doping $n_d = 6.0 \times 10^{12}$ cm^{-2} (Fig. 2b), we note that for the BG setup the on-set of transmission is shifted to lower energies compared to the TG one, resulting in the larger current. The main scattering takes place at the junction between the electrode and MoS_2 channel. This can be seen from the voltage drop in Fig. 3 where the drop is smaller at the S (positive) compared to the D (negative) electrode for the BG setup while it is about symmetric for the TG one. This indicates that more negative charge accumulates in the channel in the BG setup.

To shed light on the reason behind the dependence of I_{SD} on the stacking configuration, we have examined the electronic structure of the device and of the heterostructure in the presence of TG/BG. Fig. 4a,b shows the projected density of states (PDOS) on the graphene and MoS_2 atoms close to the MoS_2/G electrodes for the TG and BG device setups, at V_{SD} = 0.0 V and $n_d = 6.0 \times 10^{12}$ cm^{-2}. The presence of ZZ edges in the MoS_2/G overlay regions leads to the appearance of metallic edge states[25] in the energy range corresponding to that of the Dirac cone in an infinite graphene sheet, which appear as sharp peaks in the graphene PDOS. In the non-gated device, these states are found at an energy $E - E_F = 0$ meV ($E_F = \mu_S = \mu_D$), i.e., as expected from a comparison with spin-unpolarized calculations for isolated ZZ graphene nanoribbons.[25] At $n_d = 6.0 \times 10^{12}$ cm^{-2}, the graphene is doped by electrons, as the PDOS is shifted towards negative energies by a similar amount (∼100 meV) in both the TG and BG device setups. Overall, the graphene PDOS is very similar in the TG and BG device setups, indicating that the doping in graphene does not depend on the specific device setup considered. Conversely, the MoS_2 PDOS varies considerably depending on the gate position. For the gated TG and BG configurations, the onset of the MoS_2 PDOS is shifted towards negative energies by 170 meV and 320 meV, respectively, compared to its position in the non-gated setup, $E - E_F = 615$ meV. Assuming that the Schottky barrier at the contact, Φ_B, can be can be evaluated as the difference between the Fermi level and the onset of the MoS_2 PDOS, this leads to a Schottky barriers Φ_B(TG) = 445 meV and Φ_B(BG) = 295 meV. This trend is maintained up to $n_d = 10.8 \times 10^{12}$ cm^{-2}, for which Φ_B(TG) = 365 meV and Φ_B(BG) = 165 meV.

The electronic band structures of the heterostructure are shown in see Fig. 5a,c. Notice that because we are using an orthogonal cell, the K-point in the graphene and MoS_2 hexagonal Brillouin zones falls along the X $\rightarrow \Gamma$ path of the orthogonal Brillouin zone due to band folding. Because of the weak van der Waals interaction between the graphene and MoS_2, the electronic bands in the heterostructure can be regarded essentially as the superimposition of the electronic bands of the two individual 2D components (See Fig. S2 in the Supporting

Information). An analysis of electronic bands also reveals that in the non-gated structure, the graphene Dirac point is positioned at the Fermi level E_{F}, i.e. that the graphene is not doped, and that the offset between the Dirac point and the valence band maximum of MoS_2 is $\simeq$ 1.1eV, in agreement with recent experimental measurements for monolayer MoS_2 on graphene[23] (See Fig. S2 in the Supporting Information). Due to the weak interlayer interaction, Φ_{B}, can thus be evaluated as the difference between E_{F} and the conduction band minimum (CBM) of MoS_2. For the undoped MoS_2/G interface, $\Phi_{\mathrm{B}} = 638$ meV, which is close to the value obtained for the non-gated device setup and also with accurate G_0W_0 calculations.[26,27]

An intuitive picture of the dependence of Φ_{B} on the stacking sequence can be drawn by examining the electronic density redistribution induced by gating in the MoS_2/G heterostructure:

$$\Delta\rho = \rho[n_{\mathrm{d}}] - \rho[0] \tag{3}$$

Upon gating, the additional carriers accumulate in the graphene due to its metallic character. Thus, a capacitor develops in which the two plates are the graphene and the gate surface, respectively. In the BG configuration, the MoS_2 lies within the capacitor, and its electronic states are strongly affected by the capacitive electric field $\vec{E}_{\mathrm{gate}}$, as shown in Fig. 5b. This lowers the CBM of MoS_2,[28] leading to a strong decrease in Φ_{B} compared to the ungated case. The scenario differs significantly in the TG configuration as clearly seen in Fig. 5d, as $\vec{E}_{\mathrm{gate}}$ remains confined within the gate and the graphene due to the good screening properties of the latter.[29] As a consequence, $\vec{E}_{\mathrm{gate}}$ influences the MoS_2 layer only weakly, leading to a much reduced dependence of Φ_{B} on n_{d} compared to the BG case. We stress how these predictions differ qualitatively from those obtained for similar MoS_2/G heterostructures using a homogeneous electric field, which could not address the the difference between the TG and the BG setups.[30]

The Schottky barriers, Φ_{B}, calculated from the bandstructures at different n_{d} are shown in Fig. 6b. Gating the heterostructure leads to an overall decrease of the Schottky barrier,

Φ_B. This decrease is considerably faster for the BG configuration than for the TG one. Indeed, at $n_d = 6.0 \times 10^{12}$ cm^{-2}, which correspond to applied gate voltages V_G(BG) = 2.27 V and V_G(TG) = 2.03 V, Φ_B(BG) = 275 meV and Φ_B(TG) = 432 meV. At $n_d = 10.8 \times 10^{12}$ cm^{-2}, which correspond to applied gate voltages V_G(BG) = 4.09 V and V_G(TG) = 3.70 V, Φ_B(BG) = 88 meV and Φ_B(TG) = 356 meV (See Fig. S7 in the Supporting Information for a plot of Φ_B *vs.* V_G). As a result, the difference $\Delta\Phi_B = \Phi_B(BG) - \Phi_B(TG)$ reaches values as high as $\Delta\Phi_B = 156$ meV at $n_d = 6.0 \times 10^{12}$ cm^{-2} and $\Delta\Phi_B = 268$ meV at $n_d = 10.8 \times 10^{12}$ cm^{-2}. This trend is perfectly consistent with that of I_{SD} *vs.* n_d, with the shift in on-set of electron transmission shown in Fig. 2b, with that of Φ_B *vs.* n_d estimated using the device PDOS, and with that of $\Delta\Phi_B$ *vs.* n_d obtained for the device electrodes (See Fig. S3 in the Supporting Information). We may estimate the ratio of the thermionic currents at $n_d = 6.0 \times 10^{12}$ cm^{-2} to be $e^{\Delta\Phi_B/k_BT} \sim 600$, in reasonable agreement with Fig. 2a.

In addition to Φ_B, the tunnelling current in the gated MoS_2/G contact depends also on the number of graphene carriers (n_G) available for injection into the MoS_2. The latter can be extracted from the relation $E_F - E_D = \hbar v_F \sqrt{\pi |n_G|}\text{sign}(n_G)$, where E_D is the energy of the Dirac point with respect to E_F and $v_F = 10^6$ m s^{-1}. Within the range of doping considered, n_G (BG) $\approx n_G$(TG), and even at $n_d = 10.8 \times 10^{12}$ cm^{-2}, the Dirac point is shifted by a similar amount in the BG and TG setups (see Fig. 5a,c and Fig. S4 in the Supporting Information). By comparing these results with those for Φ_B and with the calculated transconductance data, it can be concluded that in the range of n_d considered the position of the MoS_2 conduction band in the contact region strongly depends on the device setup, and ultimately determines the performance of the 2D-FET device.

In Fig. 6 we also compare the Φ_B *vs.* n_d data obtained with the CG method with those obtained with the HG and HG+diel. methods. The three methods yield essentially the same result for the chosen gate distance of 20 Å, the qualitative trend of Φ_B with n_d being very similar with only minor differences in the actual values of Φ_B. This indicates that encapsulation of the 2D-FET in dielectrics such as h-BN [5] does not change the generic effect

pointed out here.

The calculated barrier heights may be explained in a rather simple analysis of the band diagram as shown in the Supporting Information, where we find that the top- and back-gated barrier heights are $\Phi_{\mathrm{B}}^{\mathrm{TG}} = \Phi_{\mathrm{B0}} - (E_{\mathrm{F}} - E_{\mathrm{D}})$ and $\Phi_{\mathrm{B}}^{\mathrm{BG}} = \Phi_{\mathrm{B0}} - (E_{\mathrm{F}} - E_{\mathrm{D}}) - e^2 n_{\mathrm{G}} d/\varepsilon_0$, respectively; here Φ_{B0} is the barrier height at zero doping density and $d \simeq 1.7$ Å is the distance between graphene and the first sulphur layer in MoS_2. It follows that the barrier height difference $\Delta\Phi_{\mathrm{B}} = \Phi_{\mathrm{B}}^{\mathrm{TG}} - \Phi_{\mathrm{B}}^{\mathrm{BG}} = e^2 n_{\mathrm{G}} d/\varepsilon_0$ is increasing linearly with doping density in agreement with Fig. 6c. These results can also be applied to structures, where MoS_2 is replaced by another 2D-material with a significant bandgap.

In conclusion, we have performed first principle DFT-NEGF calculations on a MoS_2 device contacted by graphene showing how the contact resistance between overlayed graphene electrodes and the 2D semiconductor is very sensitive to the position of the gate. This points out a novel design rule for future electronic devices based on stacked heterostructures.

Methods

The structure of the 5×5/4×4 hexagonal supercell used to construct the MoS_2/G heterostructure (see main text) was optimized using VASP.[31] The ionic cores were described using the projector augmented wave (PAW) method.[32] The kinetic energy cutoff for the plane waves expansion was set to 400 eV. The Brillouin zone was sampled with a 3×1×3 Monkhorst-Pack (MP) grid[33] together with a 50 meV Methfessel-Paxton[34] smearing. The electronic exchange-correlation energy was described using the Perdew-Burke-Ernzerhof (PBE)[21] exchange-correlation (xc) functional. Dispersion interactions were accounted for by using the semiempirical DFT+D2 method by Grimme.[22] The vacuum gap between the periodic repetitions of the heterostructure in the Z direction was set to 20 Å. During the structural optimization, the center of mass of the system was fixed by freezing the positions of the molybdenum atoms, while the sulfur and graphene atoms were allowed to fully relax. The geometry was optimized until the forces on the moving atoms were lower than 0.05 eV/Å.

The orthogonal MoS_2/G cell used to simulate the heterostructure was constructed starting from the optimized geometry of the 4×4/5×5 MoS_2/G hexagonal cell. For these calculations, the SIESTA[18] code was used. We used the PBE xc functional and a 15×1×21 MP grid together with a Fermi function corresponding to an electronic temperature of $k_BT = 25$ meV. Troullier-Martin[35] norm-conserving pseudo potentials were used to describe the ionic cores. The energy cutoff for the real space grid used to calculate the Hartree and xc contribution to the total energy was set to 200 Ry. A DZP (SZP) basis-set was used for graphene (MoS_2), together with an energy shift of 200 meV. The electronic band structure obtained with these settings is very similar to that obtained from plane-waves calculations using VASP (see Fig. S5 in the Supporting Information). The vacuum gap along the Z direction was set to 120 Å. Dipole corrections in the direction normal to the MoS_2/G plane were used in the calculations of the gated heterostructure (see main text).

The armchair-oriented MoS_2/G transistor geometry (984 atoms) was obtained by repeating the MoS_2/G electrodes along the X Cartesian direction and removing the central graphene region to create the MoS_2 channel. The resulting zig-zag graphene edges where saturated using hydrogen atoms. In the finite-bias DFT-NEGF transport calculations using TRANSIESTA,[16] similar computational parameters to those employed for the heterostructure were used. The k-points grid was set to 1×3 and was increased to 1×25 for the evaluation of the electronic transmission and current. The device electrodes were calculated using a 100×1×3 MP grid. While the precise value of the Schottky barrier at a given value of n_{d} depends on the k-point sampling, this k-point grid yields a similar trend in $\Delta\Phi_{\mathrm{B}}$ as that calculated using the $15 \times 1 \times 21$ k-point grid (see Fig. S3 in the Supporting Information). Dipole corrections were employed in the calculations of the gated transistor (see main text).

In the calculations of the heterostructure using the ATOMISITX TOOLKIT,[19] we have used similar computational parameters as those of the SIESTA calculations. Mixed (Dirichlet+Neumann) non-periodic boundary conditions were in the direction normal to the heterostructure plane. Also in this case, The electronic band structure obtained with these

settings is very similar to that obtained using VASP (see Fig. S5 in the Supporting Information).

Acknowledgement

The authors thank Dr. F. Pizzocchero, L. Gammelgaard, B. S. Jessen, K. Stokbro and Profs. P. Bøggild, K. S. Thygesen for discussions. The Center for Nanostructured Graphene (CNG) is sponsored by the Danish Research Foundation, Project DNRF103. DS acknowledge support from the HCØ DTU-COFUND program.

Supporting Information Available

The following files are available free of charge.

- Transfer characteristics of the zig-zag oriented device setup
- Projected electronic structure of MoS_2/G
- Relation between $\Delta\Phi_B$ density and doping density in the MoS_2/G electrodes
- Relation between doping density and shift of the Dirac point of graphene
- Electronic structure of bulk MoS_2/G with different DFT codes
- Consistency of the electrical potential in the DFT and DFT+NEGF simulations
- Schottky barriers for the TG and BG setups of MoS_2/G *vs.* gate voltage
- Analytical model of the gated MoS_2/G vdW stack

This material is available free of charge via the Internet at `http://pubs.acs.org/`.

References

(1) Novoselov, K. S.; Mishchenko, A.; Carvalho, A.; Neto, A. H. C. *Science* **2016**, *353*, 9439.

(2) Dean, C. R.; Young, A. F.; Meric, I.; Lee, C.; Wang, L.; Sorgenfrei, S.; Watanabe, K.; Taniguchi, T.; Kim, P.; Hone, K. L. S. J. *Nature Nanotech.* **2010**, *5*, 722.

(3) Kim, K. S.; Zhao, Y.; Jang, H.; Lee, S. Y.; Kim, J. M.; Kim, K. S.; Ahn, J.-H.; Kim, P.; Choi, J.-Y.; Hong, B. H. *Nature* **2009**, *457*, 706.

(4) Wang, L.; Meric, I.; Huang, P. Y.; Gao, Q.; Gao, Y.; Tran, H.; Taniguchi, T.; Watanabe, K.; Campos, L. M.; Muller, D. A.; Guo, J.; Kim, P.; Hone, J.; Shepard, K. L.; Dean, C. R. *Science* **2013**, *342*, 614.

(5) Cui, X.; Lee, G.-H.; Kim, Y. D.; Arefe, G.; Huang, P. Y.; Lee, C.-H.; Chenet, D. A.; Zhang, X.; Wang, L.; Ye, F.; et al., *Nat. Nanotech.* **2015**, *10*, 534.

(6) Liu, Y.; Wu, H.; Cheng, H.-C.; Yang, S.; Zhu, E.; He, Q.; Ding, M.; Li, D.; Guo, J.; Weiss, N. O.; Huang, Y.; Duan, X. *Nano Lett.* **2015**, *15*, 3030.

(7) Yu, L.; Lee, Y.-H.; Ling, X.; Santos, E. J. G.; Shin, Y. C.; Lin, Y.; Dubey, M.; Kaxiras, E.; Kong, J.; Wang, H.; Palacios, T. *Nano Lett.* **2014**, *14*, 3055.

(8) Lee, G.-H.; Cui, X.; Kim, Y. D.; Arefe, G.; Zhang, X.; Lee, C.-H.; Ye, F.; Watanabe, K.; Taniguchi, T.; Kim, P.; Hone, J. *ACS Nano* **2015**, *9*, 7019.

(9) Krasnozhon, S. B. D.; Kis, A. *ACS Nano* **2013**, *4*, 3246.

(10) Roy, K.; Padmanabhan, M.; Goswami, S.; Sai, T. P.; Ramalingam, G.; Raghavan, S.; Ghosh, A. *Nat. Nanotech.* **2013**, *8*, 826.

(11) Georgiou, T.; Jalil, R.; Belle, B. D.; Britnell, L.; Gorbachev, R. V.; Morozov, S. V.;

Kim, Y.-J.; Gholinia, A.; Haigh, S. J.; Makarovsky, O.; Eaves, L.; Ponomarenko, L. A.; Geim, A. K.; Novoselov, K. S.; Mishchenko, A. *Nat. Nanotech.* **2013**, *8*, 100.

(12) Yu, Y.-J.; Zhao, Y.; Ryu, S.; Brus, L. E.; Kim, K. S.; Kim, P. *Nano Lett.* **2009**, *9*, 3430.

(13) Yang, H.; Heo, J.; Park, S.; Song, H. J.; Seo, D. H.; Byun, K.-E.; Kim, P.; Yoo, I.; Chung, H.-J.; Kim, K. *Science* **2012**, *336*, 1140.

(14) Papior, N.; Gunst, T.; Stradi, D.; Brandbyge, M. *Phys. Chem. Chem. Phys.* **2016**, *18*, 1025.

(15) Tian, T.; Rice, P.; Santos, E. J. G.; Shih, C.-J. *Nano Lett.* **2016**, *16*, 5044.

(16) Brandbyge, M.; Mozos, J.-L.; Ordejón, P.; Taylor, J.; Stokbro, K. *Phys. Rev. B* **2002**, *65*, 165401.

(17) Papior, N.; Lorente, N.; Frederiksen, T.; García, A.; Brandbyge, M. *Computer Physics Communications* **2016**, *212*, 8.

(18) Soler, J. M.; Artacho, E.; Gale, J. D.; García, A.; Junquera, J.; Ordejón, P.; Sánchez-Portal, D. *J. Phys. Condens. Matter* **2002**, *14*, 2745.

(19) Atomistix ToolKit version 2016.3. QuantumWise A/S (www.quantumwise.com).

(20) Choi, S.-M.; Jhi, S.-H.; Son, Y.-W. *Phys. Rev. B* **2010**, *81*, 081407.

(21) Perdew, J. P.; Burke, K.; Ernzerhof, M. *Physical Review Letters* **1996**, *77*, 3865.

(22) Grimme, S. *J. Chem. Theory Comput.* **2006**, *27*, 1787.

(23) Pierucci, D.; Henck, H.; Avila, J.; Balan, A.; Naylor, C. H.; Patriarche, G.; Dappe, Y. J.; Silly, M. G.; Sirotti, F.; Johnson, A. T. C.; Asensio, M. C.; Ouerghi, A. *Nano Lett.* **2016**, *16*, 4054.

(24) Ma, Y.; Dai, Y.; Guo, M.; Niu, C.; Huang, B. *Nanoscale* **2011**, *3*, 3883.

(25) Son, Y.-W.; Cohen, M. L.; Louie, S. G. *Nature* **2006**, *444*, 347.

(26) Jin, C.; Rasmussen, F. A.; Thygesen, K. S. *J. Phys. Chem. C* **2015**, *119*, 19928.

(27) Note how the present choice of lattice constant leads to an excellent agreement of the present value of Φ_B with that obtained using the G_0W_0 method in Ref. 26, as the actual value of Φ_B depends on the in-plane strain of the individual graphene and the MoS_2 layers, see Ref. 26.

(28) Zibouche, N.; Philipsen, P.; Heine, T.; Kuc, A. *Phys. Chem. Chem. Phys.* **2014**, *16*, 11251.

(29) Stokbro, K.; Petersen, D. E.; Smidstrup, S.; Blom, A.; Ipsen, M. *Phys. Rev. B* **2010**, *075420*, 82.

(30) Liu, X.; Li, Z. *J. Phys. Chem. Lett.* **2015**, *6*, 3269.

(31) Kresse, G.; Furthmüller, J. *Phys. Rev. B* **1996**, *54*, 11169–11186.

(32) Blöchl, P. E. *Phys. Rev. B* **1994**, *50*, 17953.

(33) Monkhorst, H. J.; Pack, J. D. *Phys. Rev. B* **1976**, *13*, 5188.

(34) Methfessel, M.; Paxton, A. T. *Phys. Rev. B* **1989**, *40*, 3616–3621.

(35) Troullier, N.; Martins, J. L. *Phys. Rev. B* **1991**, *43*, 1993.

Figures

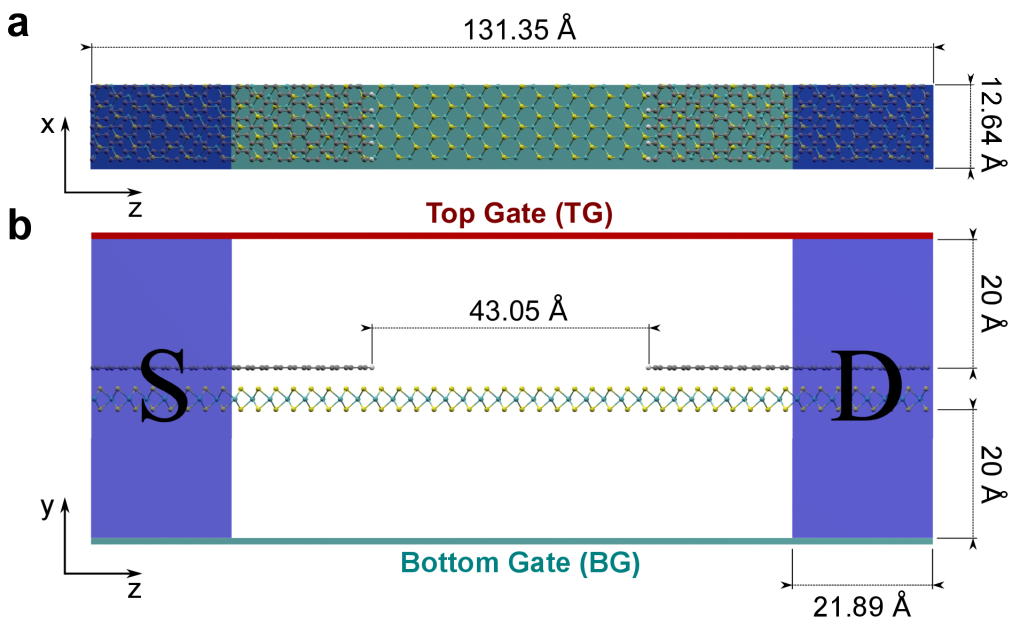

Figure 1: (Color online) Top (a) and side (b) view of the 2D-FET device setup used in the DFT-NEGF calculation. The semi-infinite MoS_2/G overlay regions used as source (S) and drain (D) electrodes are highlighted in blue. The electrostatic planar top (TG) and bottom (BG) gates used to modulate the total charge in the structure are shown in red and turquoise, respectively.

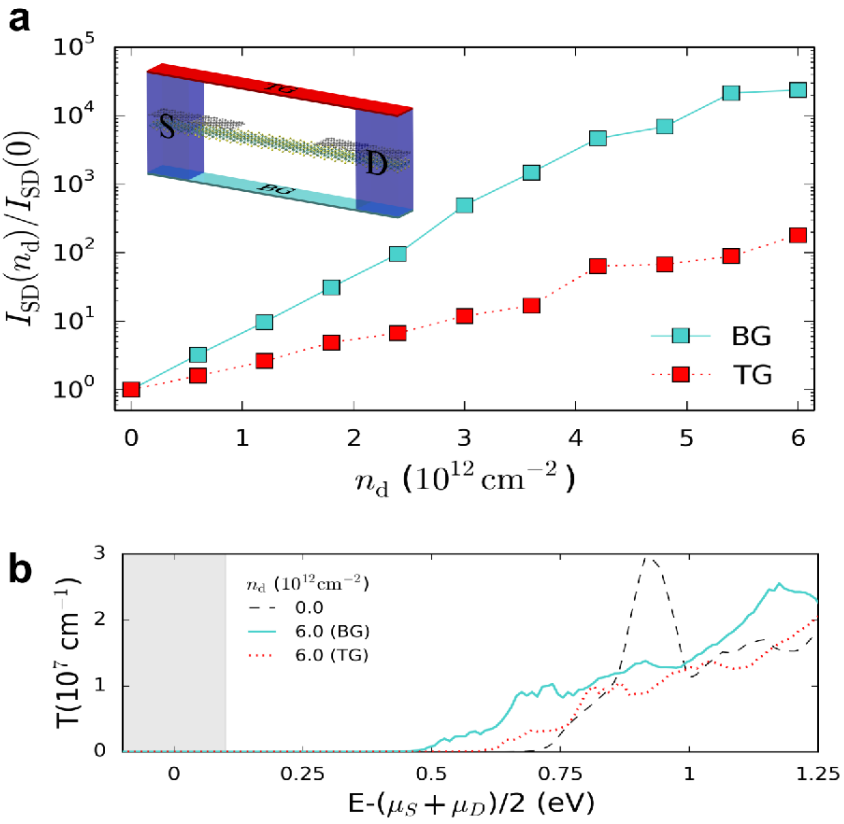

Figure 2: (Color online) (a) Source-drain current I_{SD} for the bottom-gated (turquoise, solid line) and top-gated (red, dotted line) device at source-drain bias $V_{\mathrm{SD}} = 0.2\,\mathrm{V}$, as a function of the doping level n_{d}. Inset: scheme of the device setup including the bottom gate (BG, turquoise) and top gate (TG, red). Carbon, Sulfur and Molybdenum atoms are shown in gray, yellow and cyan, respectively. The regions corresponding to the semi-infinite source (S) and drain (D) electrodes are shown as blue semi-transparent volumes. (b) Transmission spectra at $V_{\mathrm{SD}} = 0.2$ V and $n_{\mathrm{d}} = 6 \times 10^{12}$ cm^{-2} for the TG (turquoise, solid line) and BG (red, dotted line) device setup. The black dashed line corresponds to the non-doped case. μ_{S} and μ_{D} are the chemical potentials of the source and the drain electrode, respectively.

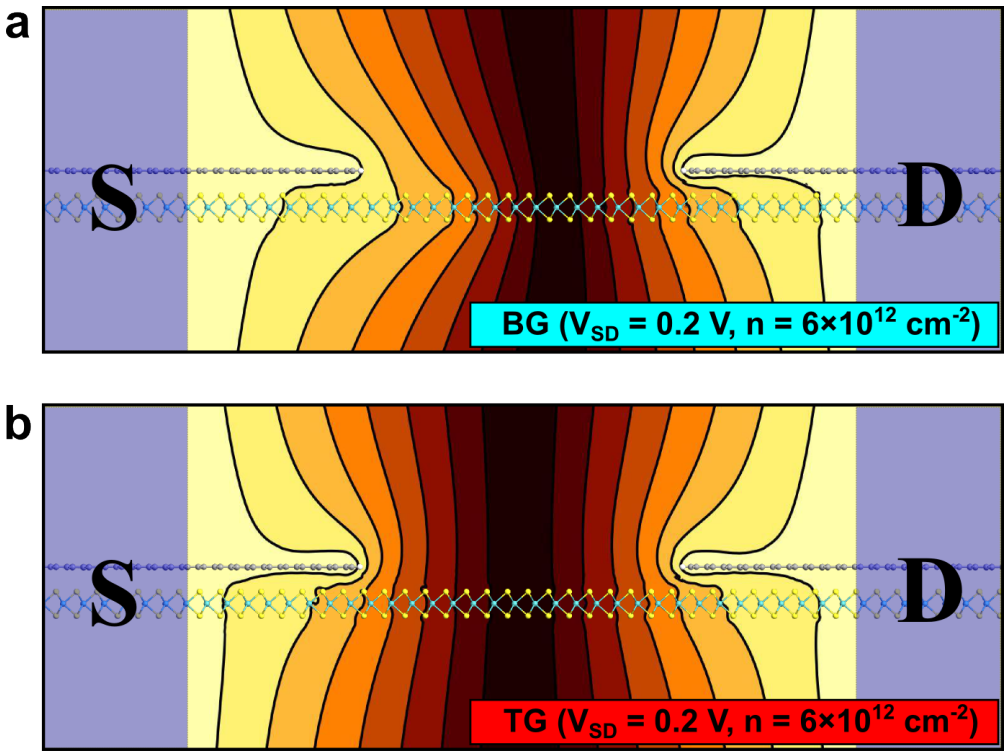

Figure 3: (Color online) 2D map of electrostatic potential drop at V_{SD}= 0.2 V and n_d = 6 $\times$ 10^{12} cm^{-2} for the BG (a) and TG (b) device setups. The data have been averaged along the X direction. For clarity, the map shows only the absolute value of the potential. Bright (dark) regions indicate regions of high (low) potential. The shaded blue regions indicate the S/D electrodes. Electrons move from S (left) to D (right). The contourlines are separated by 1.3$\times$$10^{-2}$ V.

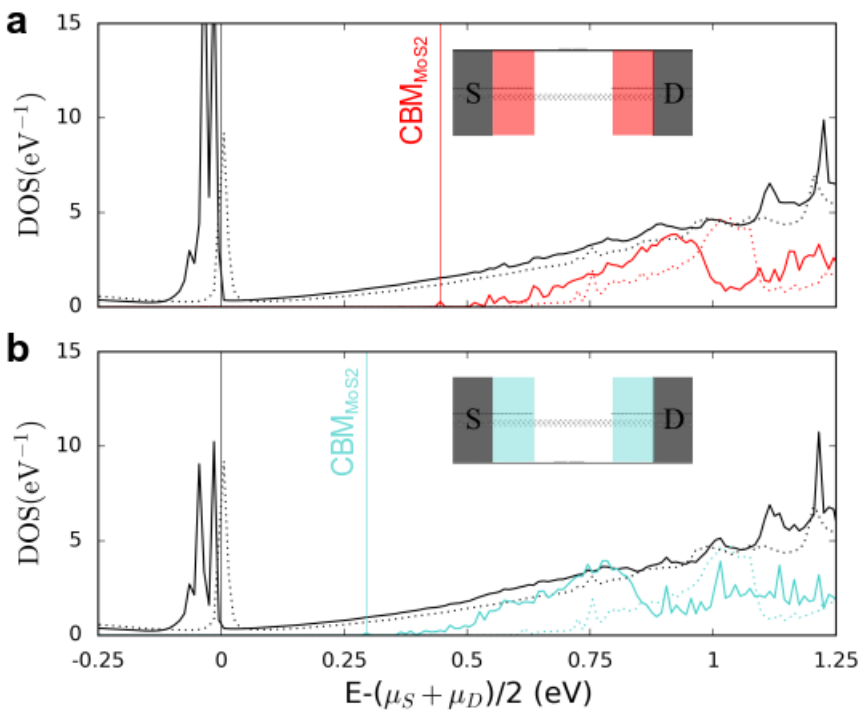

Figure 4: Projected density of states (PDOS) of the device setup at V_{SD}= 0.0 V and n_d = 6×10^{12} cm^{-2}. (a) PDOS onto the graphene (black) and MoS_2 (red) atoms of the overlay region close to the electrodes for the TG setup. The region over which the PDOS has been calculated is indicated by the red area in the inset. The vertical black (red) dashed line indicate the Fermi energy (the conduction band minimum of MoS_2). (b) PDOS onto the graphene (black) and MoS_2 (turquoise) atoms of the overlay region close to the electrodes for the BG setup. The region over which the PDOS has been calculated is indicated by the turquoise area in the inset. The vertical black (turquoise) dashed line indicate the Fermi energy (the conduction band minimum of MoS_2). In (a,b) μ_S and μ_D are the chemical potentials of the source and the drain electrode, respectively, and the PDOS on the C atoms has been multiplied by a factor 50.

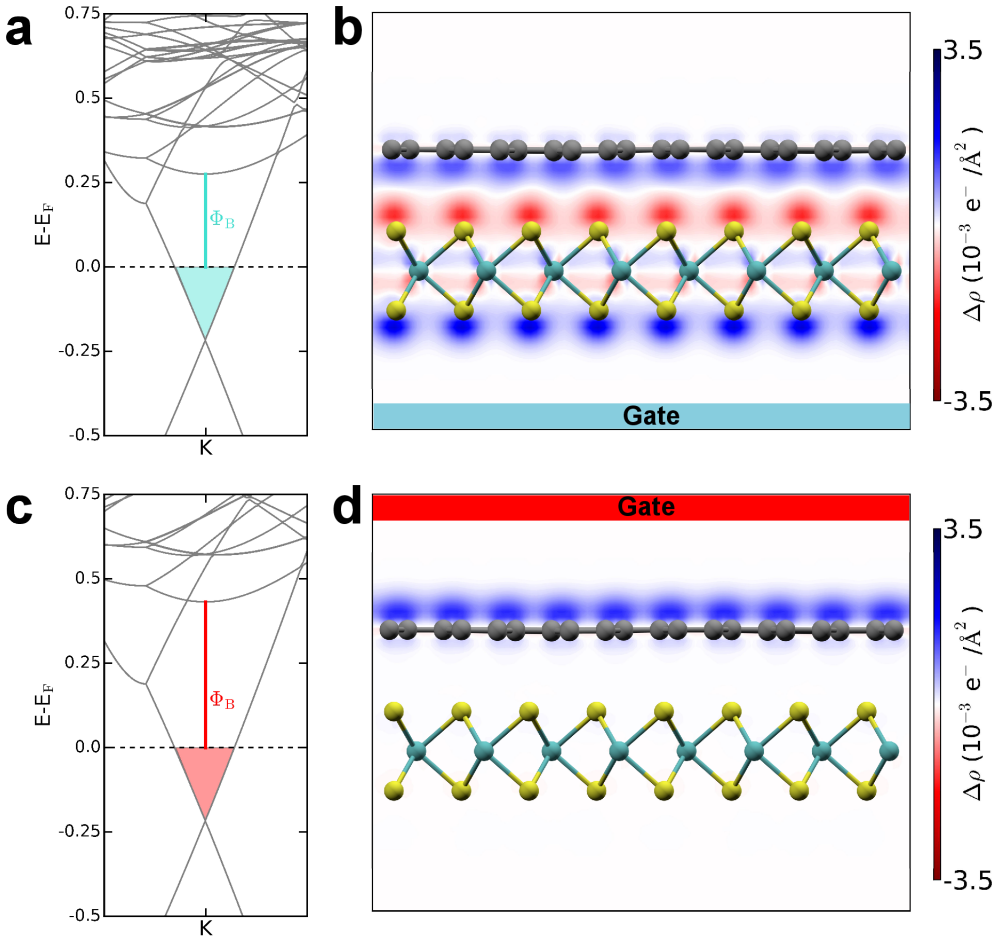

Figure 5: (a) Electronic band structure around the K-point for the BG setup of the heterostructure at $n_d = 6.0 \times 10^{12}$ cm^{-2}. The energy on the Y-axis is scaled with respect to the Fermi energy E_F. The Schottky barrier is indicated by the turquoise solid line. The shaded turquoise area indicates the portion of the graphene π^* band below the Fermi energy. (b) Electronic density redistribution $\Delta\rho$ in the BG electrode configuration at $n = 6.0 \times 10^{12}$ cm^{-2}. $\Delta\rho$ has been integrated along the electrode short axis parallel to the graphene plane. Blue and red colors indicate electron accumulation and depletion, respectively. (c,d) Same as (a,b), but for the TG electrode setup.

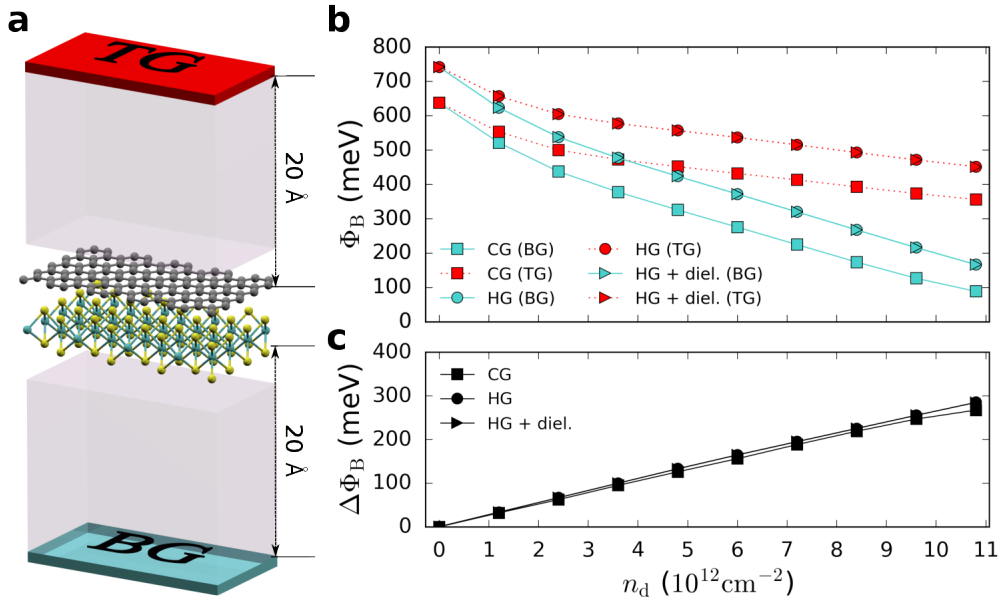

Figure 6: (a) Geometry of the MoS_2/G heterostructure, including the bottom gate (BG, turquoise), the top gate (TG, red) and the dielectric region (purple). Carbon, sulfur and molybdenum atoms are shown in gray, yellow and cyan, respectively. (b) Schottky barrier height Φ_B as a function of n_d for the bottom-gated (BG, solid lines) and top-gated (TG, dotted lines) MoS_2/G heterostructure calculated using SIESTA (squares), ATK (circles) and ATK including a dielectric region with $\kappa = 4\epsilon_0$ to mimic encapsulation in hBN (triangles). (c) Difference in the Schottky barrier height $\Delta\Phi_B$ as a function of n_d.